

5-1-1999

The Rheology and Microstructure of Concentrated, Aggregated Colloids

Leo Silbert

Southern Illinois University Carbondale, lsilbert@physics.siu.edu

J R. Melrose

R C. Ball

Follow this and additional works at: http://opensiuc.lib.siu.edu/phys_pubs

© 1999 by The Society of Rheology, Inc. Published in *Journal of Rheology*, Vol. 43, No.3, May/June 1999.

Recommended Citation

Silbert, Leo, Melrose, J R. and Ball, R C. "The Rheology and Microstructure of Concentrated, Aggregated Colloids." (May 1999).

This Article is brought to you for free and open access by the Department of Physics at OpenSIUC. It has been accepted for inclusion in Publications by an authorized administrator of OpenSIUC. For more information, please contact opensiuc@lib.siu.edu.

The rheology and microstructure of concentrated, aggregated colloids

L. E. Silbert^{a)} and J. R. Melrose

*Polymers & Colloids Group, Cavendish Laboratory, University of Cambridge,
Madingley Road, Cambridge, CB3 0HE, United Kingdom*

R. C. Ball

*Department of Physics, University of Warwick, Coventry, CV4 7AL,
United Kingdom*

(Received 9 September 1998; final revision received 21 January 1999)

Synopsis

The rheology of concentrated, aggregated colloidal suspensions is determined through particulate simulations. Aggregating systems experience a large viscous enhancement over nonaggregating systems, this being due to the increase in the component of the viscosity arising from the repulsive colloid (thermodynamic) forces when attractive forces are present. The shear behavior of aggregating systems, for colloid volume fraction $0.47 \leq \phi_c \leq 0.57$, is characterized in the steady state regime over a wide range in shear rate, and is found to be power law, shear thinning $\eta \sim f(\phi_c) \dot{\gamma}^{-\alpha}$, where the shear thinning index $\alpha = 0.84 \pm 0.01$. The effect of volume fraction enters as $f(\phi_c) = (1 - \phi_c / \phi_{\max})^{-1}$, with $\phi_{\max} = 0.64$, the value of random close packing; similarly, the viscosity also scales with the potential well depth as a power law, of index α . Associated structural features which emerge as a result of the imposed shear are identified with the rheology. The shear thinning regime crosses over into a state of ordered phase flow at high shear rates likewise simulations of hard sphere fluids. We also show that the high-shear ordered configurations appear to be a function of colloid concentration, with a transition from string phase order through to layered phases as ϕ_c increases. © 1999 The Society of Rheology. [S0148-6055(99)00603-3]

I. INTRODUCTION

Flowing colloids exhibit a wide range of phenomena that are of scientific and technological importance. Recent theoretical treatments, focusing on model hard sphere systems experiencing weak shear flows [Lionberger (1998)], have made progress at reproducing experimental and simulation data. For the case of concentrated systems, such issues become increasingly difficult to study analytically due to the intrinsic many-body nature of the system. Computer simulations allow us to study these systems, albeit a reduced version thereof, and hence help to shed light on the details concerned with the flow properties of concentrated suspensions. The most beneficial aspects come from the elucidation of the micro-rheological and microstructural behavior of the constituent macro

^{a)} Author to whom all correspondence should be addressed. Electronic mail: lesilbe@sandia.gov. Present address: Sandia National Laboratories, MS 1349, Albuquerque, New Mexico 87185.

particles making up the suspension under flow. A knowledge of this behavior is still very much unknown in detail especially at high working concentrations, as is the case in this study.

There has been an extensive effort in the study of model hard sphere systems over a range of volume fractions ϕ_c , from the dilute to the concentrated ($\phi_c \geq 0.40$) regimes. From a simulation point of view, many definitive works exist, including [Phung *et al.* (1996)], for example, among others. However, although the shear behavior of aggregated systems also continues to be studied through both experimental techniques [Patel and Russel (1987), de Rooij *et al.* (1993)] and computer modeling [Melrose and Heyes (1993), Wessel and Ball (1992), Potanin and Russel (1996), Potanin *et al.* (1995), Chen and Doi (1989)], most of these simulations have been performed at low-moderate concentrations, lower than of interest here, and largely neglect the effects of hydrodynamic interactions between the colloidal particles. We have previously reported three-dimensional (3D) simulations of concentrated systems that include hydrodynamics and aggregating forces [Silbert *et al.* (1997)]. Likewise, simulations in two dimensions (2D) have been performed [Bilodeau and Bousfield (1998)]. Buscall *et al.* (1993) carried out experimental investigations on the rheology of depletion-flocculated suspensions at $\phi_c = 0.40$, whereas Verduin *et al.* (1996) and Rueb and Zukoski (1997) probed the structure of “colloidal-gel” systems, volume fraction circa 25%, using light-scattering techniques.

In our earlier study [Silbert *et al.* (1997)] we tested our simulation model over variations in a parameter space of particle motions for an idealized, concentrated, aggregated suspension composed of monodisperse, spherical particles. The model included hydrodynamic interactions between the colloidal spheres in an approximation appropriate at high concentrations: the hydrodynamic interactions are dominated by lubrication modes between close approaching spheres. We compared results with varying approximations to the hydrodynamic model: simulations just with squeeze interactions and free particle rotations, and simulations with shear lubrication and coupled particle rotations. In addition, we switched Brownian forces on or off. Results for viscosity with shear terms were 10%–20% higher than those with just squeeze terms, while at intermediate shear rates Brownian forces lowered the results by some 20%. We validated our results against existing experimental data on the shear flow of depletion-flocculated suspensions at $\phi_c = 0.40$.

Here we restrict much of the following study to a model with squeeze hydrodynamics only, neglecting the additional shear terms and Brownian forces. This restriction plays no qualitative role on the final results [Silbert *et al.* (1997)]. We introduce the simulation model in the next section. Here we summarize the simulation technique, together with a brief introduction to the colloid forces (aggregating and repulsive terms). However, a more thorough discussion of the technique can be found elsewhere [Ball and Melrose (1997), Silbert *et al.* (1997)].

In the Results section we expound those points left open in the previous paper with an in-depth discussion on the steady state behavior of the normal stresses and the structural implications of these results, including simulation-generated intensity data $I(\mathbf{k})$ that provide us with a time-averaged determination of structural effects in the shear thinning regime as well as at high shear rates. We cover a wider range in ϕ_c , finding universal rheology persists to very high concentrations and over many decades in shear rate. Presently we are unable to simulate at very low shear rates and the first Newtonian plateau due to computational restrictions, and therefore report findings for intermediate to high shear rates.

We determine the functional dependence of the viscosity on the colloid volume fraction, and we also explore the effect of the aggregating potential, which enables us to provide a full constitutive relation that characterizes the rheology of our model system in the shear thinning regime. A brief look at the transient behavior of the flow is also given. A (cautious) comparison is made with experimental scattering data, showing that our simulations share some qualitative features with experiment. We end with a discussion of our findings.

II. SIMULATION METHOD

A. Equations of motion

The simulation modeling essentially comprises a version [Ball and Melrose (1997)] of Stokesian dynamics [Bossis and Brady (1984), Durlofsky *et al.* (1987)] which enables the study of concentrated colloidal systems by incorporating Lees–Edwards boundary conditions [Lees and Edwards (1972)] on arbitrarily large, defined by the computational box volume Ω , periodic cells. We define the hard core colloid volume fraction, $\phi_c = (\pi/6)\rho d^3$ of N particles of diameter d , with particle number density $\rho = N/\Omega$. In considering time scales long with respect to the viscous momentum relaxation time of the suspension, we treat the particles at the Langevin/Smoluchowski level and the fluid by the creeping flow equations. Stick boundary conditions are imposed on the fluid at the particle surfaces.

The equations of motion for N such particles immersed in a Newtonian fluid with viscosity μ thus express a quasistatic force balance

$$\mathbf{F}^H + \mathbf{F}^P + \mathbf{F}^B = \mathbf{0}. \quad (1)$$

The $6N$ force/torque vectors are: (i) hydrodynamic forces \mathbf{F}^H , exerted on the particles due to their relative motions in the presence of the solvent, (ii) colloidal forces \mathbf{F}^P (the sum of repulsive and attractive terms), and (iii) Brownian forces \mathbf{F}^B .

The terms \mathbf{F}^H and \mathbf{F}^B have approximate representations and their detailed expressions are available elsewhere [Ball and Melrose (1997), Silbert *et al.* (1997)]. In the version of Stokesian dynamics of [Bossis and Brady (1984), Durlofsky *et al.* (1987)] a low moment mobility tensor is combined with lubrication terms in the resistance tensor. In a concentrated system, however, we argue that \mathbf{F}^H is dominated by lubrication hydrodynamic terms between the close approaching surfaces of the colloidal spheres. This leads to a more approximate form for the hydrodynamic interactions in which the resistance matrix is two body and short ranged. Note that the inversion of this resistance matrix does give a long ranged, many-body mobility matrix. We suggest that at high concentrations ($\phi_c > 0.40$) the additional long ranged parts lead only to small improvements. The truncated algorithm used here involves only the inversion of sparse matrices and is faster, $O(N^{1.5})$ rather than $O(N^3)$, although we note that efforts continue to develop $O(N)$ versions of the algorithm of Bossis and Brady (1984), Durlofsky *et al.* (1987) [Brady (1998)].

Others are using this truncated scheme [Bilodeau and Bousfield (1998), Doi *et al.* (1987), and Toivakka *et al.* (1995)]. We discuss elsewhere the accuracy and point out the likely sources of errors in shear terms [Ball and Melrose (1997), Silbert *et al.* (1997)]. The calculation of \mathbf{F}^B is also discussed elsewhere [Ball and Melrose (1997), Bossis and Brady (1989)]

In this work, the colloid force term, \mathbf{F}^P , contains both attractive—hence the term “aggregated” colloids—and repulsive terms. We choose to model depletion aggregated colloids, that is, colloids in a mixture with nonadsorbing polymers of size R_g at volume

fraction ϕ_p (which sets the depth of the attractive well). We assume a size ratio 1:10 between the polymer to colloid diameters (i.e., $R_g/d = 0.1$, this sets the range of the attractive force), and in the pseudo one-component, macrofluid approximation, we therefore model the aggregating forces \mathbf{f}^{dep} on the Asakura–Oosawa (AO) depletion potential [Russel *et al.* (1991)]. This has recently been measured for the case of colloid+polymer mixtures near a wall [Rudhardt *et al.* (1998)], though recent work has highlighted the limitations of the AO potential [Götzelmann *et al.* (1998)].

In the AO approximation, the depletion force $\mathbf{f}_{ij}^{\text{dep}}$ acting between two colloid particles with a center–center separation $r_{ij} = |\mathbf{r}_{ij}|$ (the unit vector \mathbf{n}_{ij} points from i to j) is given by

$$\mathbf{f}_{ij}^{\text{dep}} = -\mathbf{n}_{ij} \frac{Qk_B T}{d} [\mathcal{L}^2 - (r_{ij}/d)^2] H(\mathcal{L}d - r_{ij}) \quad (2)$$

and is determined by the step function $H(x)$. \mathcal{L} depends on the size ratio R_g/d as $\mathcal{L} = 1 + R_g/d$ and sets the range of the attractive forces; the interaction strength Q (which determines the depth of the potential well), depends on the polymer volume fraction ϕ_p as

$$Q = \frac{3}{2} \frac{\phi_p}{(R_g/d)^3}. \quad (3)$$

A short range repulsive force \mathbf{f}^{rep} is also included at the surface of the spheres. This takes on the form of a Hookean spring force mimicking the osmotic part of an attached/adsorbed polymer layer. The spring coat thickness, δ_c , sets how much the thermodynamic size of the particle exceeds the hydrodynamic size, and the strength of the spring (which sets the maximal force the spring can supply before collapse) is parameterized by the dimensionless stiffness F_0 which is given the value 10^4 throughout this study.

We emphasize the significance of including this short range force in the context of our flow simulations. This issue has been extensively and correctly addressed by [Dratler and Schowalter (1996)]. Computationally, the surface coats are necessary to avoid particle overlaps, even though our simulations incorporate variable time steps. However, there are clear physical reasons for the inclusion of a repulsive colloid force term. For the case of sterically stabilized or depletion aggregating colloidal systems, colloid particles usually include some form of steric barrier to avoid irreversible coagulation in the deep van der Waals primary minima. Perfectly smooth, here we denote as “bare,” particles do not exist, although simulations of this pathological case of bare hard spheres have been carried out [Melrose and Ball (1995)]. Such systems never reach a steady state flow and jam after finite strain [Farr *et al.* (1997)].

The resulting repulsive force $\mathbf{f}_{ij}^{\text{rep}}$ on particle i due to the near approach of j , with center–center separation r_{ij} is

$$\mathbf{f}_{ij}^{\text{rep}} = \begin{cases} -\mathbf{n}_{ij} [F_0 - (F_0/2\delta_c)(r_{ij} - d)] & \text{for } r_{ij} - d < 2\delta_c \\ \mathbf{0} & \text{for } r_{ij} - d > 2\delta_c. \end{cases} \quad (4)$$

The resulting interaction potential is shown in Fig. 1, and may be thought of as the colloidal equivalent of a Lennard-Jones system. This potential is characterized by the values of certain parameters defined in the simulation. These parameters, together with their typical values, are summarized in Table I.

Although we restrict our study to this particular functional form of the interaction potential, we believe that in this one-component, macrofluid approximation, the form of

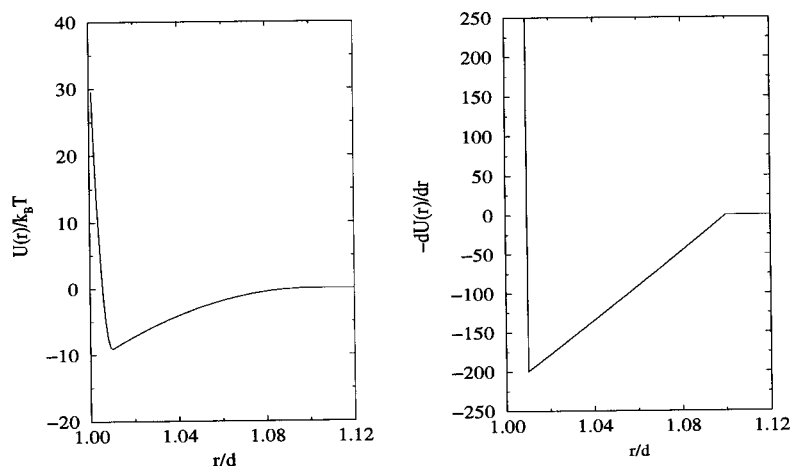


FIG. 1. Interparticle colloid pair-potential $U(r)$, and force law $-dU(r)/dr$, with the following set of parameters; polymer concentration parameter $\phi_p = 0.7$, size ratio $R_g/d = 0.1$, polymer coat thickness $\delta_c = 0.005d$.

the interaction potential, so long as it resembles Lennard-Jones-type potentials, will not give rise to qualitative differences. Though we suspect that differences might be observed in the rheology if the attractive forces (and the repulsive terms for that matter) act over distances of order the colloid size. We have performed simulations with different repulsive terms (based on a more realistic model for a surface polymer layer) [Silbert (1998)] from which the rheology data were seen to qualitatively match our previous studies using Hookean springs, and have concluded that the Hookean spring force we use here, although crude, captures the essential physics of the surface steric interactions.

The size of the cubic simulation box has side length $L = \Omega^{1/3}$. To provide a reasonable study of rheology and structure we study systems with $N = 200$, and 700 corresponding to $L \simeq 6$, and 9, respectively. We have also performed simulations over a wider range of system sizes, showing that even in the limit of very large systems ($N = 4000$), in rectangular boxes, the results are quantitatively identical. It is only in small systems, say $N \leq 50$, $L \leq 4$, that system size effects show up in the rheology. We reason that the smallness of the box in small- N simulations interferes with the microstructural mechanisms that give rise to the observed rheology [Silbert (1998)].

TABLE I. Typical simulation parameters which characterize the model system and the values they are given in many of the following studies.

Parameter	Value
Colloid volume fraction ϕ_c	0.50
Number of particles N	200
Surface layer thickness δ_c/d	0.005
Size ratio R_g/d	0.10
Polymer volume fraction ϕ_p	0.70
Potential well-depth $U_{\min}/k_B T$	9.0

B. Computation of the stress tensor

In the computation, the bulk stress of the suspension is computed as the sum over nearest-neighbor, interacting particle pairs i and j . We define nearest-neighbor pairs through a neighbor list defined on a three-dimensional tetrahedral Delaunay mesh. The vertices on the mesh define the positions of the particle centers, and consequently the mesh edges define particle separations. With this rule, all particles whose centers lie closer than $\sqrt{2}$ (diameters $d = 1$ in the simulation) are neighbors. (We point out that due to this procedure some nearest neighbors will occasionally be slightly beyond the lubrication approximation range, however, we still employ the approximate hydrodynamic terms regardless.)

Thus the stress is given by

$$\sigma = -\frac{1}{\Omega} \sum_{\alpha} \sum_{ij} \mathbf{f}_{ij}^{\alpha} \mathbf{r}_{ij} + \sigma^B, \quad (5)$$

where the edge vector \mathbf{r}_{ij} is the center-center vector separation from particle i to its neighbor j , and the sum over α is the sum over the various colloid and dissipative forces \mathbf{f}_{ij}^{α} . The Brownian contribution to the stress σ^B is detailed elsewhere [Ball and Melrose (1997), Bossis and Brady (1989)]. Normalization is with respect to the volume of the computational box Ω .

In simple shear, the apparent viscosity η at a given shear rate $\dot{\gamma}$ is given by

$$\eta(\dot{\gamma}) = \sigma_{xy}(\eta, \dot{\gamma}) / \dot{\gamma}, \quad (6)$$

where the xy component of σ represents the shear gradient-flow element of the stress tensor. It is convenient to normalize η with respect to the solvent viscosity μ , and so we define the relative viscosity $\eta_r = \eta / \mu$.

The total viscosity η_r itself may be decomposed into contributions arising from the force components where η_r^H and η_r^B denote the hydrodynamic and Brownian contributions to the relative viscosity, and the interparticle colloid force contribution to the viscosity η_r^P , comes from the sum of the repulsive component η_r^{PR} and the attractive component η_r^{PA} [compare this notation with Eq. (1)].

We measure the imposed shear rate in terms of the accepted nondimensional shear rate the Peclet number. In the simulations, the units are chosen so that the particle diameter d , the solvent viscosity μ , and the thermal energy $k_B T$, Boltzmann's constant times the absolute temperature, are numerically equal to unity. We define the Peclet number, Pe , as

$$Pe = \frac{\dot{\gamma} d^3 \mu}{k_B T}. \quad (7)$$

In these units, therefore, Pe is the shear rate. Consequently, time is measured in units of $d^3 \mu / k_B T$ and force in units of $k_B T / d$.

Although most of our simulations do not include Brownian forces, we nevertheless insist on measuring the shear rate in units of Pe , although it is not strictly correct to do so. Our previous studies [Silbert *et al.* (1997)] on model variations, that compare systems with and without Brownian forces, show that the inclusion of Brownian forces plays no qualitative role in determining the rheology of such systems.

For simulations without Brownian forces, a typical (variable) time step at $Pe = 1.0$ is $\Delta t \approx 3 \times 10^{-4}$ (i.e., $\approx 3 \times 10^3$ iterations to reach unit strain) in units where the shear rate and the particle diameter are both set equal to unity. A simulation of 700 particles

running for 2×10^5 iterations takes just a few hours on a standard workstation. For simulations that do include Brownian motion, the time step is generally reduced, and at $Pe = 1.0$, $\Delta t \approx 2 \times 10^{-5}$. Time steps vary approximately linearly with shear rate.

III. RESULTS

A. Steady state rheology

Concentrated aggregated suspensions form gel- or glassy-like structures when allowed to equilibrate without shear. Brownian dynamics simulations have been used to study the stress-strain transient regime of model particle gels, see West *et al.* (1994) and more recently Whittle and Dickinson (1997). Such systems are strictly metastable, and can remain in an aggregated state for time scales which far exceed the times of the simulation studies. Therefore, with regards to our simulations, crystallization or irreversible coagulation is not observed when at rest. However, the effects of the imposed shear will change the nature of these colloidal systems as will be shown throughout this work. One can imagine that the states which are not observed when no shear is applied are frustrated, but can either be enhanced or conversely suppressed when the shear is switched on.

The following studies are solely concerned with the steady state behavior of flowing colloids. It is thus necessary to ensure that the collected data are taken beyond the transient regime so that any memory/start-up effects are erased. The notion of the steady state regime with respect to the simulations can be realized after a time, measured in units of strain γ , at which the bulk system has reached a state of dynamic equilibrium. Loosely, we can define this state as the point in the simulation at which the fluctuations in the sampled viscosity diminish (and hence the associated errors are minimized), and a constant viscosity with time is attained.

Figure 2 compares the temporal behavior of the viscosity at $Pe = 1.0$ for two different starting configurations. The first start-up sequence uses a Monte Carlo (MC) generated hard sphere configuration (denoted by the solid diamonds in Fig. 2) where the shear and the aggregating forces are switched on at the same time. This sequence is characterized by an initial rise in the computed viscosity. The preaggregated start-up configuration, in which the aggregating forces and Brownian forces are switched on prior to shearing to allow the system to reach an aggregated state, is characterized by an initial fall in the viscosity (see inset to Fig. 2).

In general, Fig. 2 shows that each system undergoes a transient regime for the first part of the flow, up to $\gamma \approx 10$ for the MC curve, and $\gamma \approx 40$ for the preaggregated curve, during which the viscosity increases for the MC configuration and decreases for the aggregated configuration. However, after this transient regime, the computed viscosity reaches its steady state value. A small drift is sometimes evident, as in the data of Fig. 2, but we consider that beyond $\gamma \approx 10$ (or 40) the system has reached the steady state regime. We note that the MC configuration provides a shorter route to the steady state—almost three times quicker than for the preaggregated configuration—thus proving more convenient in reducing the computer time required to reach the steady state.

By comparing the response of the two systems, the shape of MC curve can be explained thus; when the simulation is *first* started for an initially MC hard-sphere configuration, the aggregating forces and shear are turned on together. Initially the colloids “feel” the attractive forces between them, suggesting that the initial reaction is for the particles to fall into the attractive wells provided by their neighbors. During this stage, the imposed flow, together with the attractive forces, initially gives way to large scale network formation and particle—particle bonds are being formed at a greater rate than they are broken: a transient gel-like network forms. These transient configurations are widely

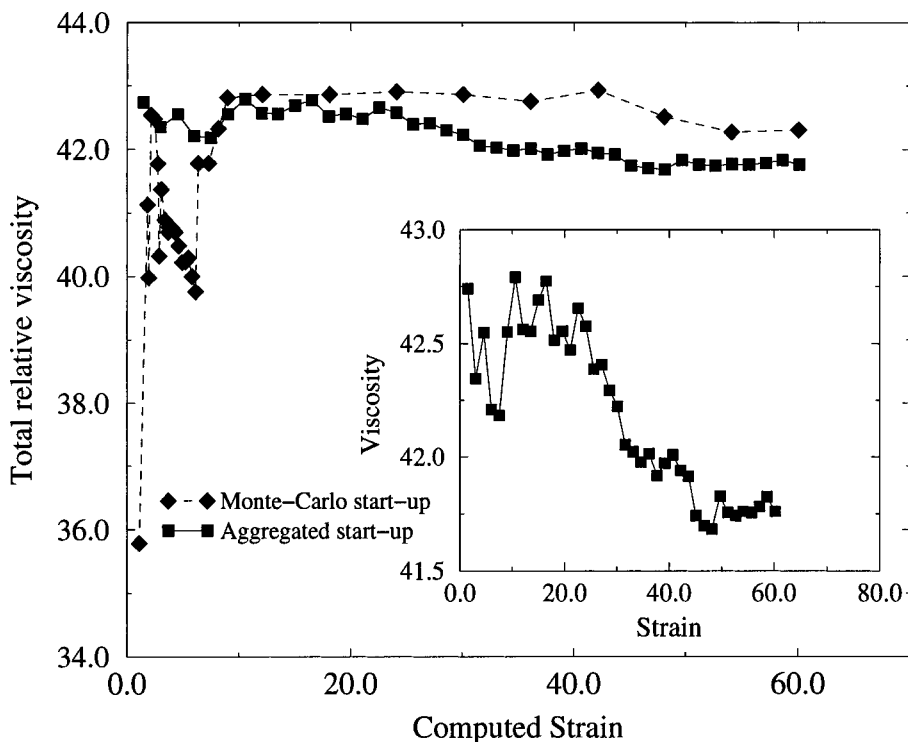


FIG. 2. Start-up transient regime at $Pe = 1.0$ for a hard-sphere Monte Carlo generated configuration (solid diamonds) and pre-aggregated rest state (solid squares). The inset shows in more detail the evolution of the pre-aggregated start-up configuration.

regarded to be different from those achieved once the system has reached the steady state [Wolthers (1997)]. Such large scale structures are likely to dominate the stress in the system in the first instance, leading to an initial sharp rise in the viscosity. With continued application of the shear, restructuring occurs in such a way that the initial large scale structures break and rupture, and hence the viscosity ceases to increase. After this stage the bond formation and breakup processes equilibrate—the steady state mechanism now dominates—giving rise to the observed steady state behavior and the viscosity levels.

B. Shear thinning

The computed rheology curves of two 200 particles systems at $\phi_c = 0.50$ are shown in Fig. 3: one with aggregating forces (with $U_{\min} = 9.0k_B T$ —we use the notation that U_{\min} is the positive value of the well depth), the other without aggregating forces (i.e., a hard sphere suspension). Both systems include hydrodynamic interactions, Brownian forces, and Hookean spring surface forces. The relative viscosity η_r is computed over many decades in the dimensionless shear rate Pe . Additional points are plotted at $Pe = 1.0$, where we have varied the strength (but not the range) of the attractive forces; $U_{\min} = 5.2k_B T$ and $2.6k_B T$. Because the stress is computed as a running average over many configurations during the simulation, the associated error bars represent noise in the steady state.

The rheology data in Fig. 3 qualitatively match experimental studies, at lower colloid concentrations, on depletion-flocculated suspensions [Buscall *et al.* (1993), Russel *et al.*

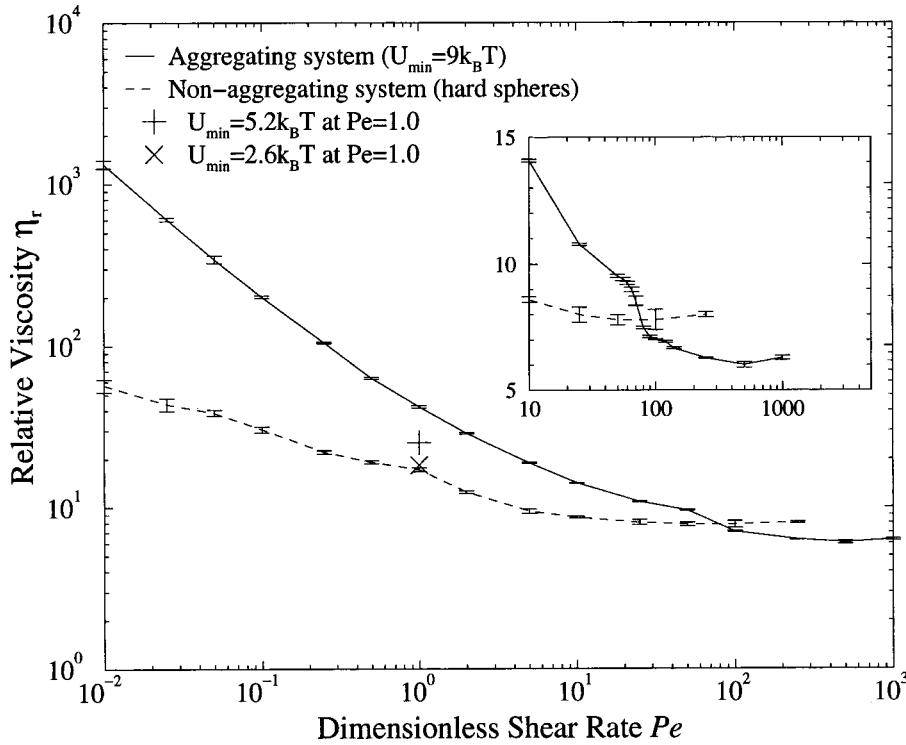


FIG. 3. Comparison of rheology between an aggregating system (with $U_{\min} = 9k_B T$) and a nonaggregating system (hard sphere model) at $\phi_c = 0.50$ and $N = 200$. All systems include a short steric coat and full hydrodynamic lubrication modes and Brownian forces. Additional points at $Pe = 1.0$ are included where we have varied the depth of the potential well. The inset shows the high shear rate region.

(1991)], as well as studies on “colloidal gels” [Rueb and Zukoski (1997), Huang and Sorensen (1996)], whereby shear thinning is seen over a large range of shear rates. However, we do not shear at low enough Pe to observe the *first* Newtonian plateau, characterized by the *zero-shear* viscosity η_0 , due to computational restrictions. To shear at lower values of Pe than shown in Fig. 3 would require an inordinate amount of computer time to reach the steady state. Thus the rheology data presented here correspond to the latter part of an equivalent experimental rheology curve [Silbert *et al.* (1997)].

In the shear thinning regime, the viscosity of the aggregating system is greatly enhanced over the nonaggregating system and this disparity becomes more pronounced the deeper the well depth (see additional points on graph). On approach to the high shear rate region $Pe > 10.0$, the viscosity of the aggregating system undergoes a transition, $10 < Pe < 100$, to a region where the viscosity eventually appears to level as it reaches the second Newtonian plateau (see inset). Before the pseudo-plateau region $Pe < 100$, the system undergoes gross structural rearrangements, although well-defined order is not yet achieved, until at $Pe = 100.0$ the particle configurations do achieve an ordered state of flow (which at this volume fraction is seen to be string phase flow as shown in Fig. 6). Experimentally, the infinite-shear viscosity η_∞ is usually determined from the value of the viscosity at the second Newtonian plateau. However, this is never truly reached in the simulations and, although the viscosity goes through a minimum

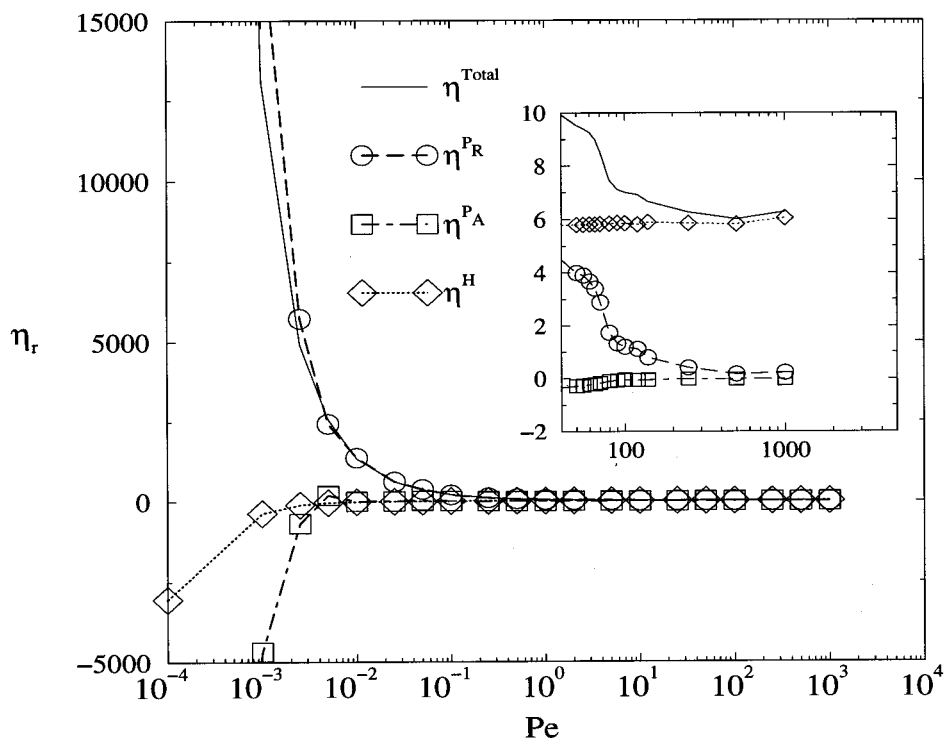


FIG. 4. Contributions to the viscosity of the aggregating system, $U_{\min} = 9k_B T$, arising from the individual forces. The inset shows the approach to high shear rates.

(from which we initially determine η_{∞}), the aggregating system eventually shear thickens at very high shear rates.

In comparison, the hard sphere system shear thins to a much milder degree than the aggregating system, and then thickens at lower shear rates. In the hard sphere case, ordering under shear occurs at much lower shear rates (before the onset of shear thickening). The presence of the attractive forces effectively inhibits the disorder–order (shear thinning–shear ordering) transition. Although we restrict our study to shear thinning and shear ordering, others have investigated the role of colloid forces on shear thickening [Boersma *et al.* (1995)].

In Fig. 4 we analyze the contributions to the total viscosity of the aggregating system by plotting the components of the viscosity arising from the force components; the colloid repulsive Hookean surface force contributes to η_r^{PR} , the colloid attractive depletion term η_r^{PA} , and the hydrodynamic force (squeeze force) η_r^H . It is only recently that progress has been made in decomposing these terms experimentally [Bender and Wagner (1995)].

In the shear thinning regime the Hookean spring surface force dominates the computed viscosity for the aggregating system. This is also true for the hard sphere system (see Table II). It is quite puzzling, at first sight, why the aggregating forces appear to contribute negligibly to the viscosity. In contrast, the common ingredient in many theories is the stretching and breaking of aggregated bonds between particles, and, although this is occurring to some degree, the results of Fig. 4 suggest that the dominant positive contribution to the total viscosity comes from the compression of close approaching

TABLE II. Total viscosity η_r and the Hookean contribution η_r^{PR} for systems at $\phi_c = 0.50$, sheared at $Pe = 1.0$. As the interaction well deepens η_r increases along with η_r^{PR} .

U_{\min}	$9 k_B T$	$5.2 k_B T$	$2.6 k_B T$	Hard spheres
η_r	39.5	25.2	17.6	16.4
η_r^{PR}	38.2	24.4	16.0	10.9

particle surfaces (though not so close that the hydrodynamic lubrication forces diverge). Bender and Wagner (1995) were able to show that the viscous response in a flowing colloidal system is due to the repulsive colloid forces. Dratler and Schowalter (1996) have also performed simulations, albeit in 2D monolayers, that predict the viscous response of a concentrated system is greatly modified when repulsive colloid forces are present.

As the interaction well deepens the total viscosity likewise increases *because* the contribution of the Hookean spring coat viscosity η_r^{PR} , also increases. Table II shows the value of the total viscosity and the contribution from the Hookean spring force [as calculated from the virial Eq. (5)] at $Pe = 1.0$ (data taken from Fig. 3). Therefore, the mechanism(s) that gives rise to the enhanced viscous response, in the shear thinning regime, experienced by those systems that include attractive forces, arises from a complex interplay between the attractive forces and the surface spring coats.

The depletion forces and the hydrodynamic forces contribute negligibly, in comparison to the Hookean term, to the computed viscosity during shear thinning. The general trend for η_r^{PA} is to become less negative with increasing shear rate, whereas η_r^H becomes less negative during shear thinning and increasingly positive as the shear rate is increased further.

Beyond the shear thinning regime, $Pe > 10$, the dominant contribution to the total viscosity now comes from the hydrodynamic component η_r^H (see inset to Fig. 4). At $Pe = 100$ $\eta_r^H \gg \eta_r^{PR} > |\eta_r^{PA}|$. This transition in viscous contributions coincides with the structural rearrangements that lead to an ordered phase (see Fig. 6) at high shear rates ($Pe \geq 100$). At these high shear rates the aggregating forces are negligible in comparison to the shear forces such that the system may be regarded as a hard sphere system and so we see ordered structures under flow (shown in Fig. 6), likewise simulations of hard spheres [Phung *et al.* (1996)]. The onset of this regime is suppressed (occurs at higher shear rates) compared to hard spheres without aggregating forces. At higher shear rates still, $Pe \geq 1000$, shear thickening is observed. The hydrodynamic contribution to the viscosity increases further and the hydrodynamically dominated flow regime gives way to hydrodynamic clustering.

In an effort to gain insight into the microstructural response of the system as it flows, we show several configuration snapshots and associated structure data below. We restrict this analysis to a system at $\phi_c = 0.50$, where the interaction potential minimum is set to $U_{\min} = 9 k_B T$. The microstructural pictures in Figs. 5 and 6 show the instantaneous particle configuration snapshots of a 700 particle system, spheres drawn *half size* for clarity, whose centers lie within the central box of the periodic system. The corresponding intensity data $I(\mathbf{k})$ at the same shear rate are also plotted to provide a comparison. Here $I(\mathbf{k})$ is generated as an ensemble average over many particle configurations and is thus to be regarded as time averaged in the steady state. In the computation of $I(\mathbf{k})$, the

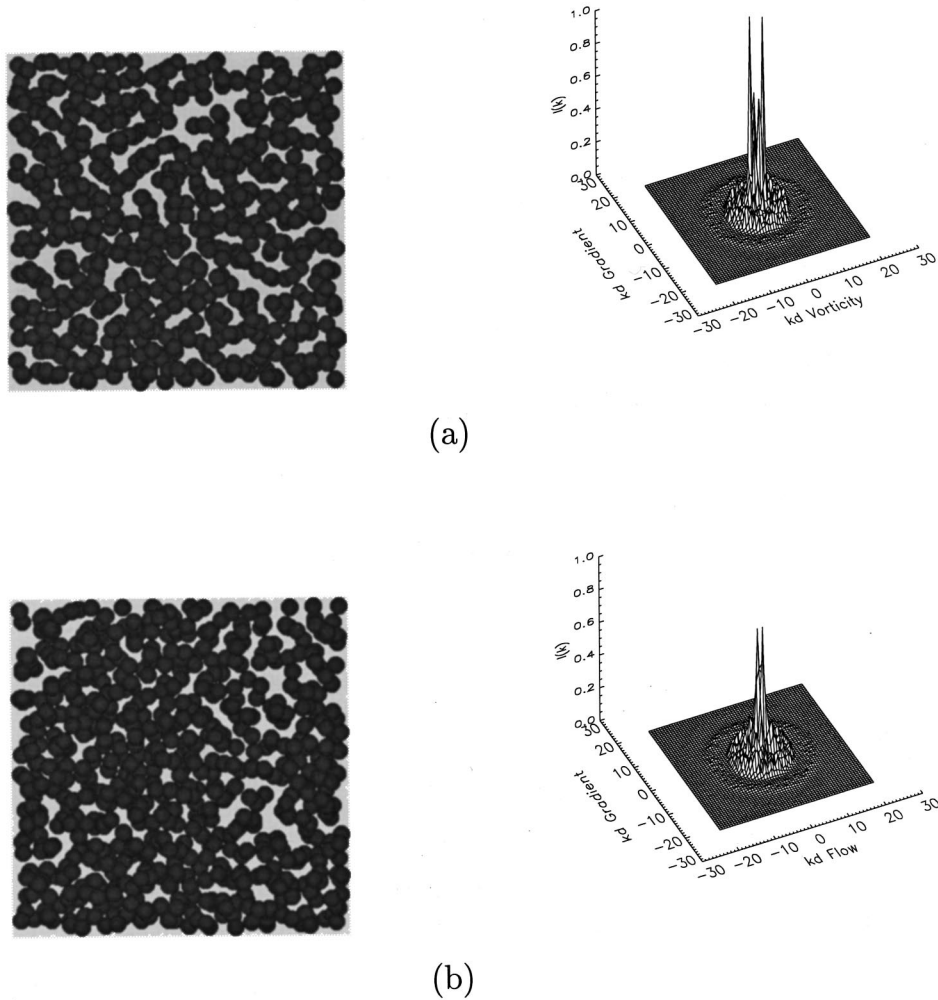


FIG. 5. Instantaneous configuration snapshot and the corresponding $I(\mathbf{k})$ of a 700 particle, $\phi_c = 0.50$, $U_{\min} = 9k_B T$, system sheared at $Pe = 0.01$, looking in; (a) the shear gradient-vorticity plane, and (b) the shear gradient-flow plane.

wave number k is restricted due to the periodic boundaries. In dimensionless units, the lowest wave number accessible is $kd \geq 2\pi/L$, for box dimension L . For a 700 particle system at $\phi_c = 0.50$, $L \approx 9.0$.

We view the data in two different directions and at two different shear rates. Figure 5 shows the snapshots and $I(\mathbf{k})$ at a low shear rate $Pe = 0.01$ —this system is undergoing shear thinning—in both (a) the shear gradient-vorticity plane (looking down the flow direction) and (b) the shear gradient-flow plane (looking down the vorticity axis). Whereas in Fig. 6 we picture a system at a high shear rate $Pe = 100.0$ in the (a) shear gradient-vorticity plane and the (b) shear gradient-flow plane.

At the lower shear rate $Pe = 0.01$ in Fig. 5, the snapshots and intensity data indicate no obvious ordering in either plane. For these concentrated systems, particle ordering is not a feature of shear thinning, and so other mechanisms must be responsible for the observed rheological behavior [Silbert (1998), Farr (1998)].

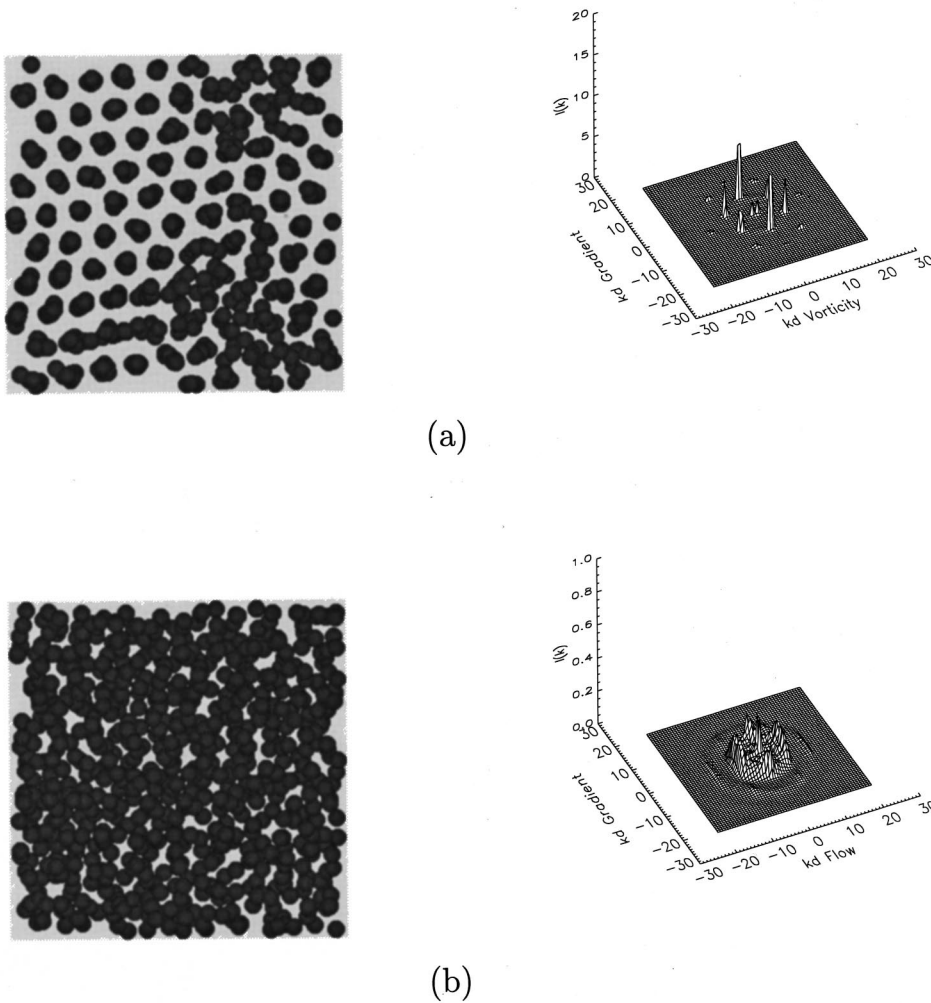


FIG. 6. Instantaneous configuration snapshot and $I(\mathbf{k})$ of a 700 particle, $\phi_c = 0.50$ system sheared at $Pe = 100.0$, looking in; (a) the shear gradient-vorticity plane, and (b) the shear gradient-flow plane.

The noticeable feature is a dominant intensity peak seen in Figs. 5(a) and 5(b). These peaks suggest correlations between particles or clusters of particles. The position of the peak lies at a lower value of k than the expected nearest neighbor, first coordination shell (usually around $kd = 2\pi$), and is commonly known as *pre peak*. However, a study of the corresponding structure factor $S(\mathbf{k})$ (not shown here) [Silbert (1998)], shows that the bulk structure takes on a form of liquid-like, short range order *plus* this pre peak.

At high shear rates, data shown in Fig. 6, the system exhibits signs of order. We see that the ordered state, a hexagonally string pack arrangement, is more clearly seen in Fig. 6(a), looking down the flow direction. The corresponding $I(\mathbf{k})$ plot correlates with this snapshot, showing the emergence of Bragg-like peaks in this plane. Although the configuration image in Fig. 6(b) does not display the same degree of ordering, $I(\mathbf{k})$ indicates that the system does show signs of order in gradient-flow plane also. The correlation ridges and peaks here are due to intra- and inter-string correlations.

Ordering under shear is known in hard sphere systems where there is some experimental evidence suggesting a regime of ordered flow [Ackerson (1990), Clarke *et al.* (1998)], and also in oscillatory shear experiments [Haw *et al.* (1998)]. Shear flow simulations of hard sphere colloidal systems [Phung *et al.* (1996)] and atomic systems [Heyes and Mitchell (1995)] report ordering at moderate to high shear rates. At high shear rates the aggregating system behaves as a hard sphere system: shear induced ordering is a feature of concentrated systems. However, we make the following qualification: shear ordering for aggregating systems appears at much higher shear rates than for equivalent hard sphere systems. Although shear ordering is a feature of concentrated colloids, the suspicion remains that the *enhanced* ordering seen in simulations in general is, in part, due to system size effects. Simulations of the high-shear behavior of electrostatically stabilized systems [Catherall (1998)] show that as the box size varies (from a simple cubic volume to a larger rectangular system), regions exhibiting different types of order develop, and the percolating string clusters, as observed in Fig. 6, actually break into separate strings for the case of longer boxes.

Nevertheless, the calculations here provide indications of a shear induced disorder-order phase transition in concentrated, *aggregated* colloidal suspensions. From a theoretical point of view, the “field” is the imposed shear rate and, hence, the “order parameter” will have some dependence on this quantity. Theoretical attempts exist that model phase transitions in colloids under shear [Morin and Ronis (1996)]. These use field-theoretic techniques at a more coarse-grained level than, say, a particulate description, to characterize the order parameter and its dependence on the shear rate. However, a general understanding of these nonequilibrium transitions to order is still lacking at a more discrete level.

C. Normal stresses

If the stress tensor σ is related to an equivalent pressure tensor through, $\sigma = -\mathcal{P}$, the diagonal components of σ are only defined up to an arbitrary constant. The more useful parameters determined from experiment are linear combinations of these diagonal components—the normal stress differences. The first and the second normal stress differences, denoted by N_1 and N_2 , respectively, are defined in Eq. (8), following the usual convention (see [Barnes *et al.* (1989)], for example)

$$\begin{aligned} N_1 &= \sigma_{xx} - \sigma_{yy} \\ N_2 &= \sigma_{yy} - \sigma_{zz}. \end{aligned} \tag{8}$$

The benefit of the simulation procedure allows the exact determination of the diagonal components of the stress. Thus it is possible to understand the behavior of the σ_{ii} without resorting to inferring their behavior from related results.

N_1 and N_2 are plotted in Fig. 7, covering the full rheological range (as in Fig. 3). The values of N_1 and N_2 in the shear thinning regime fluctuate erratically close to zero, similar to the behavior in hard sphere systems [Phung *et al.* (1996)]. The inset emphasises this region. The behavior during shear thinning is rather perplexing as we have already seen that the viscosity of the aggregating system is greatly enhanced over a hard sphere system. However, the fact that N_1 remains close to zero in this regime indicates that the structures forming in the bulk are either homogeneous throughout, or, possibly, elongated rod-like structures form along the flow-compression direction.

Beyond the shear thinning regime, $Pe \geq 10$, both N_1 and N_2 go negative, indicating a transition away from pure shear thinning behavior. However, upon the onset of order at

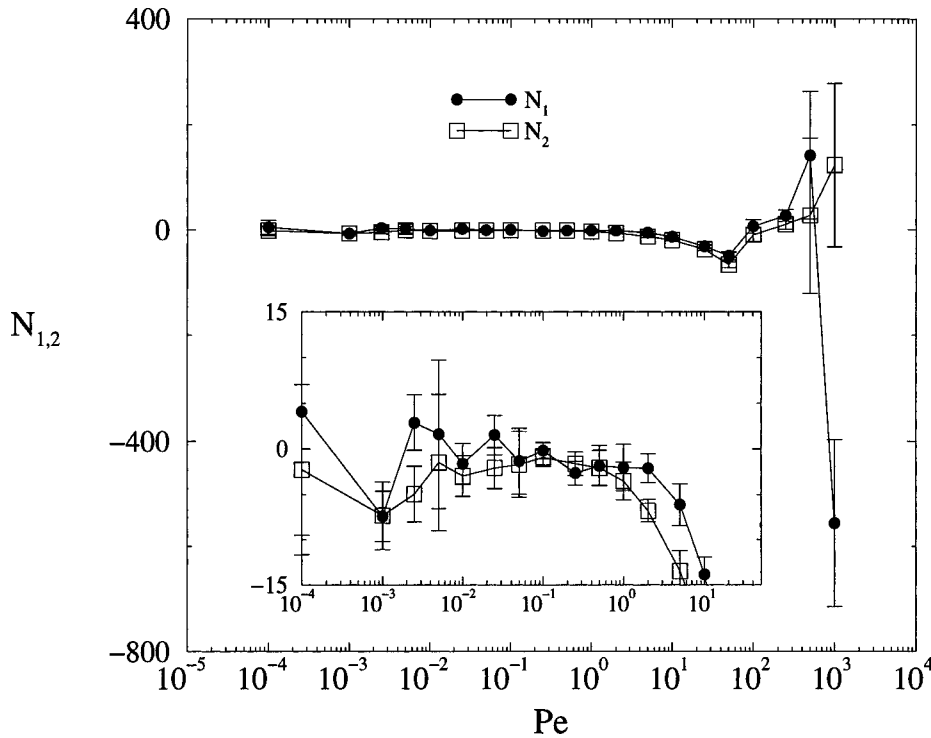


FIG. 7. N_1 and N_2 for the 200 particle system at $\phi_c = 0.50$, $U_{\min} = 9k_B T$, as a function of shear rate. The inset emphasizes the behavior during shear thinning and the gradual transition to an ordered phase at higher Pe .

higher shear rates still, $Pe > 50$, the N_k become increasingly positive until N_1 drops to a large negative value coinciding with the first signs of shear thickening.

In Fig. 8 we decompose the normal stress differences into the normal stresses, σ_{xx} , σ_{yy} , and σ_{zz} computed over the same range of shear rate as in Fig. 7. In the shear thinning regime the σ_{ii} fluctuate around zero and again, beyond the shear thinning regime, the trend is for the σ_{ii} to go negative. Consequently, the N_k also go negative because one of the σ_{ii} is more negative than the other, not because it is more positive.

From the rheology data in Fig. 3 the attractive forces do not contribute directly to the viscosity, though it is very clear that the aggregating forces are responsible, in some way, for the observed viscous enhancement. Therefore we feel it pertinent to plot the components of the normal stresses arising from the two colloid forces, the Hookean term and the depletion term [cf. Eq. (5)] denoted $\sigma_{ii}^{\text{Hookean}}$ and $\sigma_{ii}^{\text{depletion}}$, respectively (here divided by Pe). The contributions arising from the hydrodynamic squeeze force are not shown in Fig. 9 as these data are orders of magnitude smaller than the other terms. As $\sigma_{ii}^{\text{Hookean}}$ is always negative, we actually plot the magnitude, $|\sigma_{ii}^{\text{Hookean}}|$, for convenience as a direct comparison to the positive depletion contribution.

The Hookean term (which is always negative) and the depletion term (which is always positive) dominate the normal stresses in the system during the shear thinning regime even though the forces act over length scales that differ by an order of magnitude. At high shear rates the hydrodynamic squeeze term becomes comparable to the depletion term. It is through this picture that we see the relevance of the aggregating forces not previously realized from the viscosity data in Fig. 3.

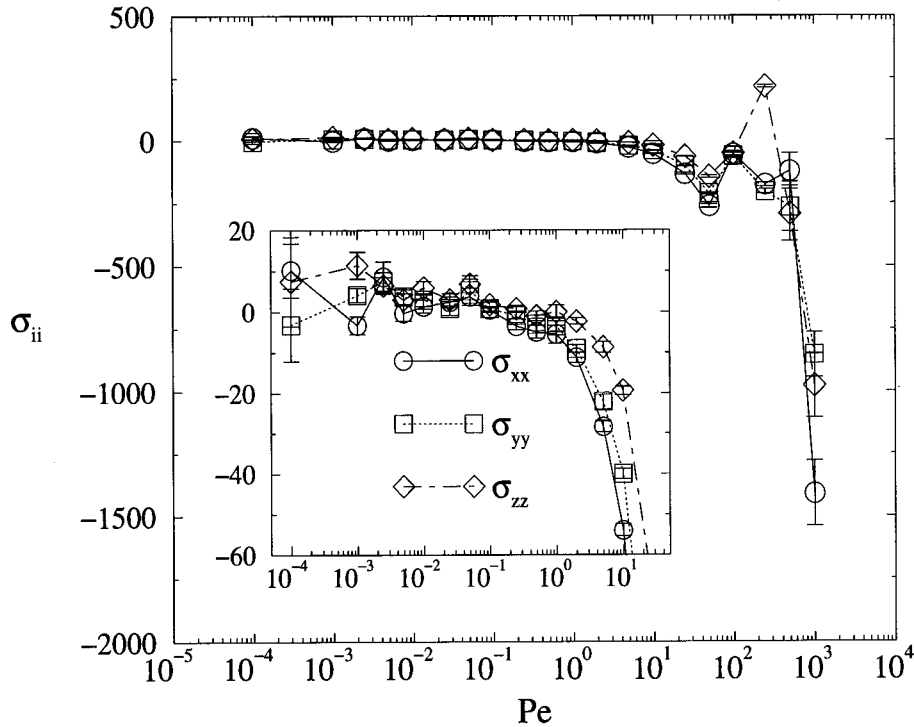


FIG. 8. The three normal stresses, σ_{xx} , and σ_{yy} , and σ_{zz} for the system at $\phi_c = 0.50$. The inset shows the shear thinning region in greater detail.

D. Viscosity dependence on volume fraction

There are several phenomenological theories purporting the dependence of the viscosity on volume fraction, many of which originate from the Einstein relation in the dilute limit [Einstein (1956)], $\eta_r(\phi_c) = (1 + 2.5\phi_c)$. Batchelor and others, see [Happel and Brenner (1983), Hunter (1992), Russel *et al.* (1991)], have made attempts to extend this relation to higher orders in ϕ_c ; however these are either restricted to the dilute regime or independently to concentrated regimes. Krieger (1972) generalized the Einstein relation in the concentrated regime, suggesting that the volume fraction dependence relies on the packing parameter p and correlates as

$$\eta_r = \frac{1}{(1 - \phi_c/p)^{[\eta]p}},$$

which reduces to the Einstein expression for an ideal, monodisperse colloidal system in the dilute limit by substituting for the *intrinsic viscosity* $[\eta] = 2.5$.

Integral pair theories for hard sphere colloids with Brownian forces have been used to obtain a functional relation [Brady (1993), Lionberger and Russel (1997)]. Generally, these suggest that the stress in the system will diverge with volume fraction like $(1 - \phi_c/\phi_{\max})^{-2}$. Here the packing parameter p is equal to the maximum packing fraction for spheres ϕ_{\max} .

In Fig. 10 the variation in viscosity is computed as a function of colloid volume fraction, $0.47 \leq \phi_c \leq 0.57$, repeated at several shear rates, $0.01 \leq Pe \leq 10.0$, with the

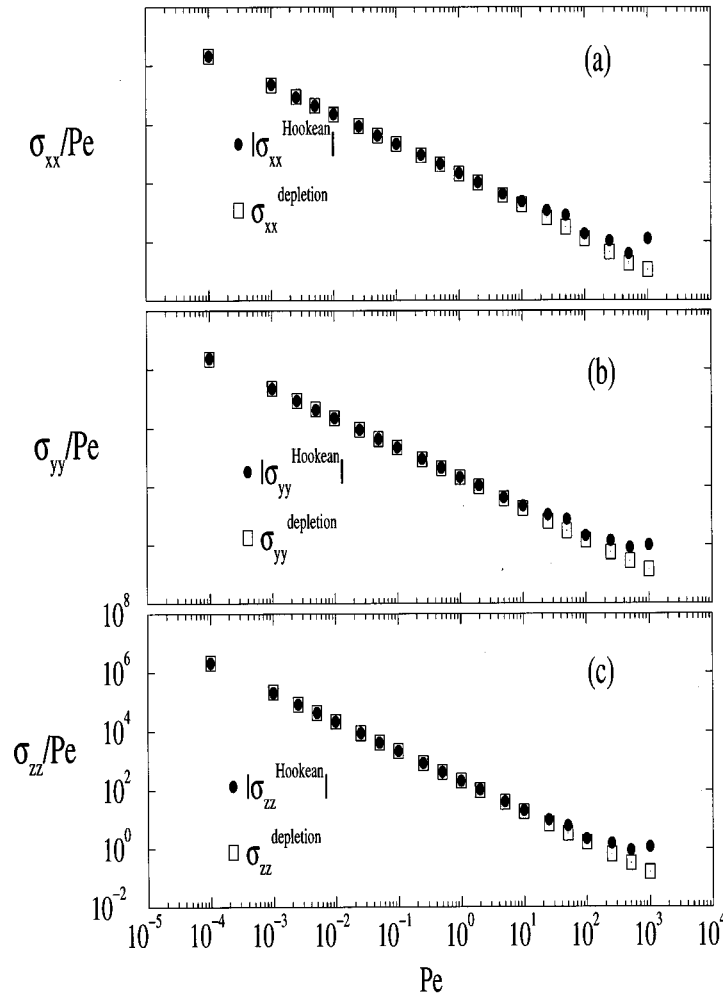


FIG. 9. The depletion contribution and the magnitude of the Hookean contribution to the stress are compared for, (a) σ_{xx} , (b) σ_{yy} , (c) σ_{zz} . Each picture has the same axes, although this is only shown in (c) for convenience.

aim of determining the functional form of the volume fraction dependence of the viscosity in the steady state, shear thinning regime. We fit each curve to the form $\eta_r = (a + b\phi_c)^{-\beta}$. The value for β which best correlates the data sets is found to be

$$\beta = 1.0 \pm 10\% .$$

Rearranging the coefficients we find that η_r can be related to ϕ_c through the following equation:

$$\eta_r(\phi_c) = \frac{k}{(1 - \phi_c / \phi_{\max})^\beta}, \quad \beta = 1.0 \tag{9}$$

and we identify the coefficient ϕ_{\max} with the volume fraction of maximum random close packing computed here to be $\phi_{\max} = 0.64 \pm 0.02$.

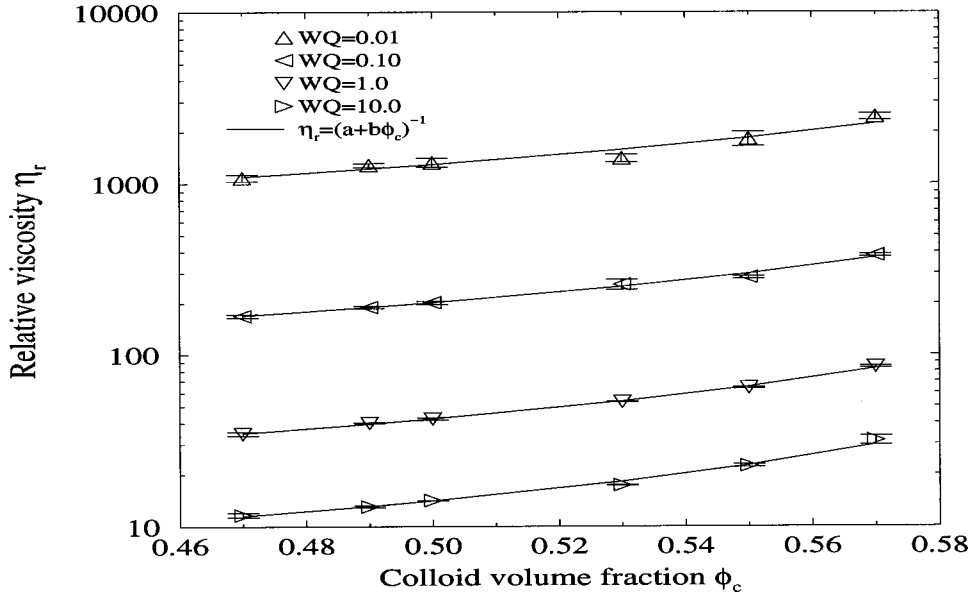


FIG. 10. Viscosity dependence on ϕ_c measured at several shear rates: $Pe = 0.01, 0.1, 1.0, 10.0$. Each data set is fitted to the curve $\eta_r = (a + b\phi_c)^{-1}$.

Although the value of $\beta = 1.0$ computed here is not the expected value as mentioned above (one might expect $\beta = 2.0$), recent work by Brady (1993) argues that in the presence of colloid forces the divergence should go like $\beta = 1.0$, though the difference between fitting either $\beta = 1.0$ or $\beta = 2.0$ is small over this range of volume fraction.

The coefficient k in the numerator of Eq. (9) is independent of colloid concentration ϕ_c , and contains the dependence on shear rate and the interaction potential (varying the potential well depth will alter the viscous response [Buscall *et al.* (1993)]. The dependence of the viscosity on the interaction potential may be characterized by the value of the depleting polymer concentration ϕ_p , or similarly the depth of the potential well U_{\min} . The potential minima U_{\min} is linear in ϕ_p , and follows an empirical relation: $U_{\min} = 13.0\phi_p$.

We also find that the scaling of the viscosity on ϕ_p is given by a power law relation

$$\eta_r(\phi_p) = \kappa' \phi_p^\lambda = \kappa U_{\min}^\lambda, \quad \lambda = 0.87 \pm .03. \quad (10)$$

Buscall *et al.* (1993) were able to provide a tentative expression based on their experimental investigations on depletion-flocculated systems at $\phi_c = 0.40$. They found that the measured viscosity similarly scales as a power law with variations in the depletent concentration.

For the pseudo Lennard-Jones-type systems we study, we feel that in the regime of interest, moderately aggregating systems, the effect of the attractive forces enter through the strength of the interaction potential and so we choose to characterize the relation Eq. (10) in terms of U_{\min} , as this allows a more general approach. The coefficient κ is found to be unity, within error, $\kappa \approx 1.0 \pm 10\%$, and so we determine the dependence Eq. (10) to be, $\eta_r(U_{\min}) = U_{\min}^\lambda$. Although we have not yet investigated, we anticipate the scaling of Eq. (10) must break down at small potentials when aggregating forces are smaller

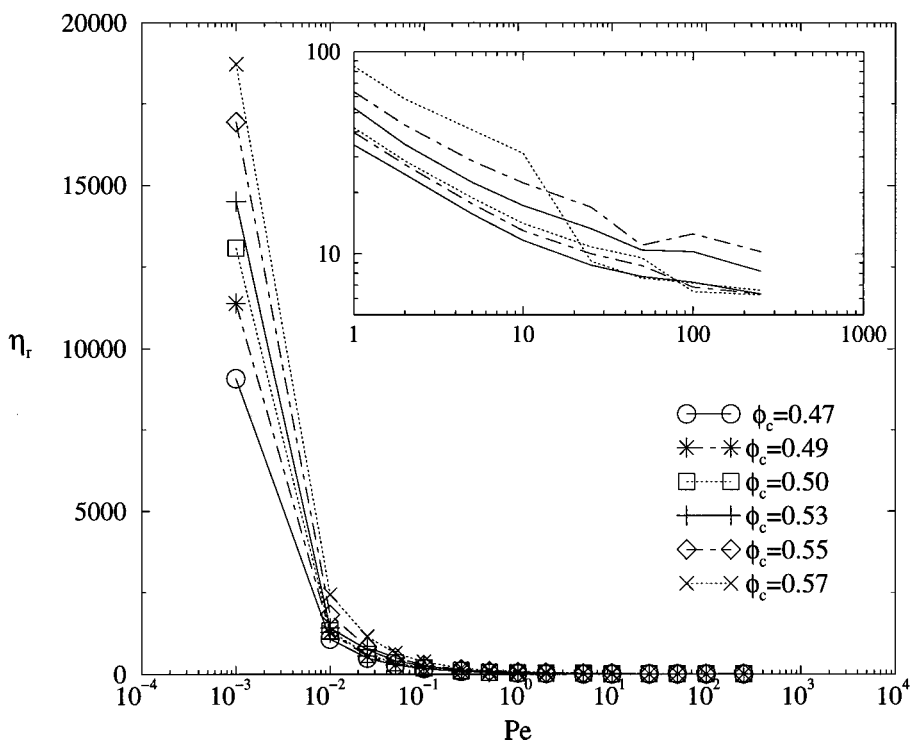


FIG. 11. Rheology of aggregated systems in the concentrated regime, $0.47 \leq \phi_c \leq 0.57$. Viscosity η_r vs shear rate Pe in dimensionless units. The inset shows the moderate-high shear rate region.

than $k_B T$, and the system and its rheology will reduce to that of hard spheres, and also at very large potentials, where the systems may effectively become glassy.

E. Power law, shear thinning colloids

The rheology of aggregated systems over a range of colloid volume fraction in the concentrated regime, $0.47 \leq \phi_c \leq 0.57$, is shown in Fig. 11. All simulations were performed on 200 particle systems ($L = 6d$), interacting through squeeze hydrodynamics (Brownian forces were switched off), Hookean spring forces, and an aggregating potential set to $U_{\min} = 9 k_B T$. As expected, all systems exhibit extreme shear thinning that extends over many decades in Pe , until apparently leveling upon the onset of the second Newtonian (pseudo-) plateau at high shear rates. However, the inset in Fig. 11 shows that there is a trend with increasing volume fraction, for the systems to display rather peculiar behavior at moderate-high shear rates. In these cases the viscosity appears to jump, quite dramatically, to lower values to such an extent that the viscosity at $Pe = 250.0$ for $\phi_c = 0.57$ is lower than that for $\phi_c = 0.47$. We attribute this anomalous behavior to shear ordering effects which become increasingly prominent at higher ϕ_c for the systems sizes simulated here. We suspect that the degree of spontaneous ordering observed here would not be so pronounced for larger systems.

The data presented in Fig. 11 show that all systems show a region of power law-like shear thinning between, say $0.001 \leq Pe \leq 10.0$. Therefore in an attempt to characterize the rheology, we find a phenomenological relation that correlates the data in the shear thinning regime. There are numerous constitutive relations, either semiempirical or phe-

TABLE III. A comparison of the ratio of the viscosities when the system is purely shear thinning $\eta_r(Pe = 0.01)/\eta_r(Pe = 0.10)$, and when the system is crossing over to an ordered state of flow $\eta_r(Pe = 10.0)/\eta_r(Pe = 100.0)$.

ϕ_c	$\frac{\eta_r(Pe = 0.01)}{\eta_r(Pe = 0.10)}$	$\frac{\eta_r(Pe = 10.0)}{\eta_r(Pe = 100.0)}$
0.47	6.4	1.61
0.49	6.8	1.9
0.50	6.6	2.1
0.53	5.5	1.7
0.55	6.5	1.8
0.57	6.4	4.4

nomenological, relating the dependence of the viscosity on the shear rate [Barnes *et al.* (1989), Hunter (1992), Russel *et al.* (1991)]. As an initial guess to describe the constitutive relation, one might expect that the rheology would obey the well-known Hershel–Bulkley relation or the Cross model [Barnes *et al.* (1989), Hunter (1992)]. However, because we do not shear at low enough shear rates we are unable to determine η_0 . An alternative relation proposed by Sisko [Barnes *et al.* (1989)], relates the measured viscosity to the shear rate and the infinite-shear plateau value

$$\eta - \eta_\infty = K\dot{\gamma}^{-\alpha}, \quad (11)$$

in which the shear thinning exponent α is defined. In this relation, however, the constant K is undetermined and is usually fitted empirically to the data. In this first instance we do not try to provide any theoretical or semiempirical justification for the fit, as used by Baxter-Drayton and Brady (1997), for example, as we are merely concerned with a purely phenomenological relation, though we do not discount the fact that other relations may be used to correlate the data.

In referring to Eq. (11), η_∞ is considered to be a well-defined value, and reflects the fact that, say, the system has reached a well-defined state of flow. However, we have seen that the simulations do not necessarily provide a reliable estimate of η_∞ . Also, from the analysis of the normal stress differences at $\phi_c = 0.50$ (see Fig. 7), it is apparent that there exists a crossover region between the power law-like, shear thinning regime and the onset of the ordered phases at high shear rates.

Clearly the shear thinning region, where the viscosity falls significantly with increasing shear rate, is due to a different rheological mechanism than the high shear region where the change in viscosity is minimal. We highlight this with the data in Table III. Therefore, the power law behavior must be differentiated from the nonpower law regime, hence we feel the value of η_∞ should be chosen to be *the equivalent infinite shear viscosity of the second Newtonian plateau if it were to be well defined* in the simulations.

Recalling that the viscosity is dominated by the contribution from the hydrodynamic forces (η_r^H in Fig. 4) at the higher shear rates, we may proceed by assuming that the systems behave as hard spheres in this high shear regime. We would therefore expect the value of η_∞ to correlate like hard spheres. de Kruif *et al.* (1985) managed to correlate η_∞ for hard sphere systems over the full range of volume fractions, relating it to ϕ_c via

$$\eta_\infty = (1 - \phi_c/0.71)^{-2}. \quad (12)$$

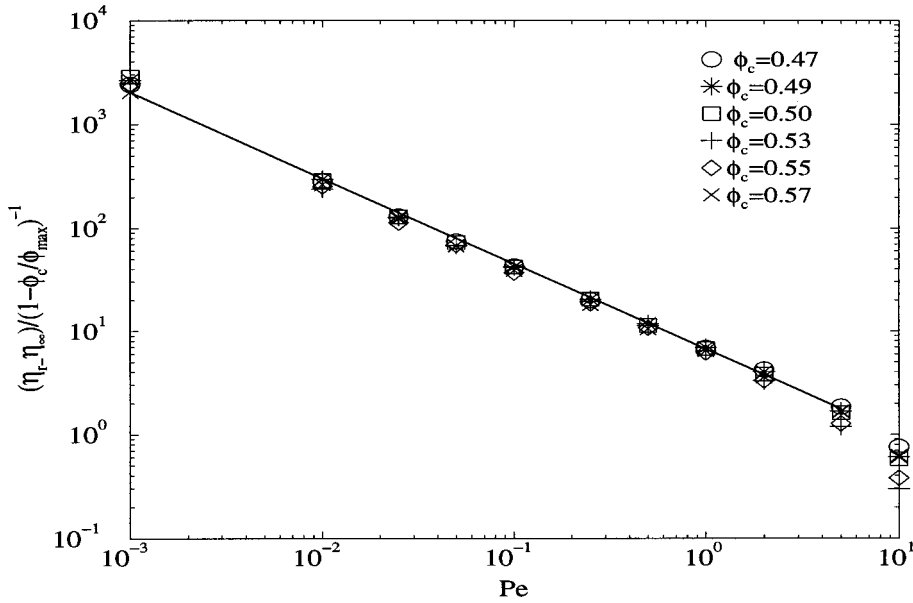


FIG. 12. Rheology data rescaled according to Eq. (13) showing approximate universal shear thinning behavior for aggregated systems in the concentrated regime: log–log plot. Slope = -0.84 ± 0.01 .

The value 0.71, assumes that the value of η_∞ derives from the well-defined flow of the systems in an ordered face-centered-cubic structure.

Using the dimensionless parameters in the simulation, the Sisko relation may be rewritten as

$$\eta_r - \eta_\infty = KPe^{-\alpha}, \tag{13}$$

such that the value of η_∞ (which is nondimensionalized) is now given by Eq. (12). The constant K , in Eq. (13), can only account for those parameters other than the shear rate: these can only be ϕ_c and the value of the interaction potential in the current study. We therefore write $K = K_1K_2$, and set $K_1 = K(\phi_c) = (1 - \phi_c/\phi_{\max})^{-1}$, and $K_2 = K(U_{\min}) = U_{\min}^\lambda$ from our previously determined quantities in Eqs. (9) and (10), respectively.

We define the power law shear thinning region to be the subset of data of the rheology curve that conforms to Eq. (13) for which η_∞ is defined in Eq. (12). Points on the rheology curve not deemed to be of power law type are then omitted from being related through Eq. (13). In rescaling the viscosity with respect to the volume fraction dependence of Eq. (9), on the log–log plot of Fig. 12, we find that the rheology data, for the majority of the shear thinning flow, collapse onto a single master curve.

Therefore in the context of our flow simulations, concentrated aggregated colloids exhibit power law, shear thinning that is universal with respect to volume fraction in the concentrated regime (up to the value of η_∞). We see that the deviation away from power law universality occurs around $Pe \approx 10.0$, the same region at which the normal stress differences in Fig. 4 also deviated from linear behavior. The rheology may thus be characterized as power law up to moderate shear rates, but there then exists a transition to a different mechanism of flow eventually leading to ordered phases at high shear rates.

The slope of the line in Fig. 12 provides the value of the shear thinning exponent α , thus fully characterizing the rheology of the fluid. The averaged value is calculated to be,

$\alpha = 0.84 \pm 0.01$. The value of this exponent is very close to the value estimated from experimental data on depletion-flocculated suspensions at $\phi_c = 0.40$ [Buscall *et al.* (1993)], where the exponent is calculated to be α [Buscall *et al.* (1993)] = 0.83. The value of α is also in the region of that obtained from shear experiments of colloidal gels, albeit at lower colloid volume fractions circa 25%, by Verduin *et al.* (1996) and similarly Rueb and Zukoski (1997), and also on the shear studies of polymer gels (aqueous gelatin) [Huang and Sorensen (1996)] (α [Huang and Sorensen (1996)] = 0.8 ± 0.05). Verduin *et al.* (1996) report the shear thinning exponent as, $\alpha = 0.77$, at weaker potentials, but dropping to 0.43 at stronger potentials. From the work by Rueb and Zukoski (1997), the shear thinning exponent can be crudely estimated to be, $\alpha \simeq 0.7$.

We highlight the fact that the value of λ is equal to α within error, and so we suggest that in this approximation $\lambda = \alpha = 0.84$. A recent kinetic model of the rheology [Farr (1998)] shows that through simple scaling arguments the viscosity should scale with the interaction potential as a power law, with the same shear thinning exponent.

We may thus write out the full (nondimensionalized) constitutive relation obeyed by our aggregated colloidal systems that is valid in the shear thinning regime

$$\eta_r(Pe, \phi_c, U_{\min}) = \frac{U_{\min}^\alpha}{(1 - \phi_c/0.64)} Pe^{-\alpha} + \frac{1}{(1 - \phi_c/0.71)^2}, \quad \alpha = 0.84 \pm 0.01, \quad (14)$$

$$N_1 = 0.0$$

$$N_2 = 0.0. \quad (15)$$

The behavior at very low shear rates remains to be studied. However, we note that a generalization of the Eyring theory has been proposed for this regime [Baxter-Drayton and Brady (1997)].

F. Ordered states at high shear rates

We also present a brief study on ordered states at high shear rates for a range of volume fractions. In Fig. 13 we view particle configuration snapshots of 200 particle systems, with the spheres drawn half size for clarity, in the range, $0.47 \leq \phi_c \leq 0.57$ sheared at $Pe = 100$. We restrict this to the high shear rate region of the rheology curve as the shear thinning regime is understood to behave independently of volume fraction.

Viewing the configurations in the gradient-vorticity plane, that is, looking down the flow direction, the system undergoes several transitions. At the lowest concentration studied $\phi_c = 0.47$ a semiordered phase exists, whereby particle strings exist in tandem with disordered regions. As ϕ_c increases, however, the hexagonally packed string phase emerges at $\phi_c = 0.50$ and further transitions occur, in an apparently continuous manner, into an intermediate string/layer phase at $\phi_c = 0.55$, finally reaching a truly ordered layered phase at $\phi_c = 0.57$.

We imagine that the geometrical constraints on such concentrated systems will eventually result in the emergence of strong ordering in all planes, and indeed we have shown here a first qualitative indication that shear induced phase transitions between ordered particle structures exist as a function of volume fraction (essentially these aggregating systems behave as hard spheres at these shear rates). Together with our earlier observations at $\phi_c = 0.50$, we expect that any theoretical considerations must take into account the dependence of shear rate *and* volume fraction when explaining the shear induced transitions in concentrated colloids. To reiterate a point of caution, since this particular study has been restricted to 200 particle systems, it is still unclear how responsive order-

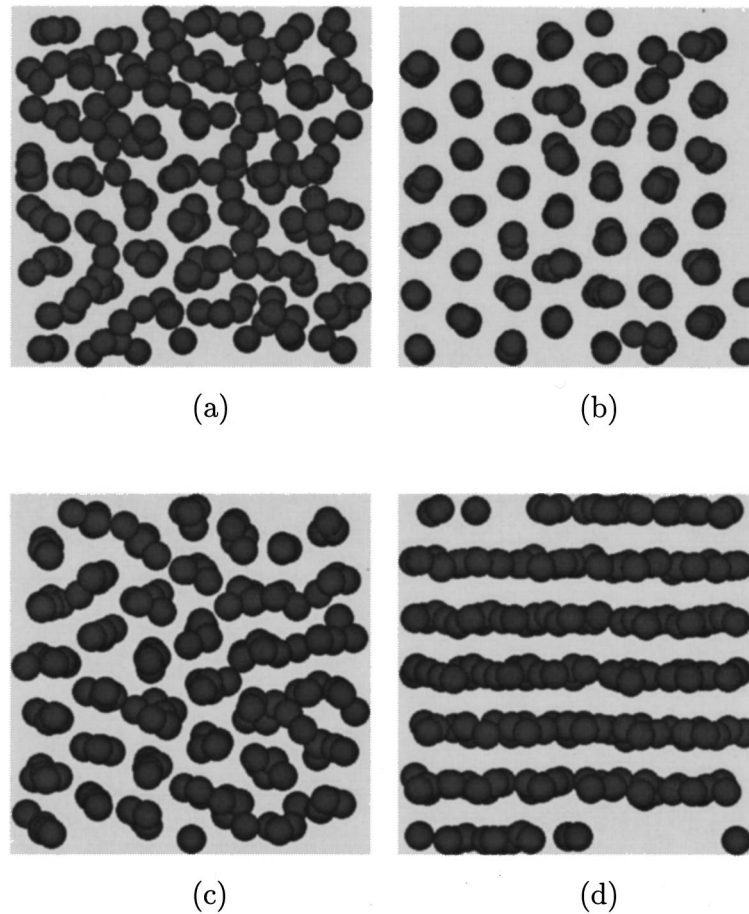


FIG. 13. Configuration snapshots of a 200 particle system looking down the flow direction sheared at $Pe = 100$ for; (a) $\phi_c = 0.47$, (b) $\phi_c = 0.50$, (c) $\phi_c = 0.55$, and (d) $\phi_c = 0.57$.

ing is to size effects. However, simulations which neglect hydrodynamic interactions observe different types of ordering consisting of gross layered phases at lower concentrations ($\phi_c = 0.30$) [Melrose and Heyes (1993)] and are deemed slightly less physically accurate.

G. Comparison with experiment

We are currently unaware of any scattering experiments on concentrated, aggregated systems under flow. The experiments by Verduin *et al.* (1996) and [Rueb and Zukoski (1997)] are concerned with colloidal gel-like systems at lower volume fractions than of interest here.

Verduin *et al.* (1996) carried out work on a system which is regarded as a model system for *adhesive hard sphere dispersions* [Verduin and Dhont (1995)]. Their system of spherical, stearyl coated, silica particles at $\phi_c = 0.25$ provides a crude comparison to the simulations presented here. We compare, with caution, structural data with our higher

volume fraction data. We have previously compared our rheology data [Silbert *et al.* (1997)] with experimental results for depletion-flocculated systems at 40% volume fraction [Buscall *et al.* (1993)].

It is still unclear how one should regard microstructures at moderate concentrations. At lower volume fractions, the system can be described in terms of open, fractal-like networks [Potanin and Russel (1996), Potanin *et al.* (1995)]. However, as the concentration increases the system becomes increasingly packed and so the notion of “open” becomes less meaningful. At $\phi_c = 0.25$ it may be more appropriate to make comparisons with the concentrated regime.

In Fig. 14 we compare the scattering data of the simulation model of an aggregating system at $\phi_c = 0.50$ ($U_{\min} = 9k_B T$) and the experimentally observed scattering pattern for a gel-forming system at $\phi_c = 0.25$. The data are viewed in the flow-vorticity plane (i.e., looking down the gradient direction). The top three fully shaded plots of $I(\mathbf{k})$ are the simulation data at $Pe = 0.05, 5.0,$ and 10.0 . The *experimental* data [reproduced from Verduin *et al.* (1996)] is shown as the (lower four) mesh plots. The shear rates may be nondimensionalized and converted into simulation units using the details of the system from Verduin *et al.* (1996): $Pe \approx 0.0, 0.07, 5.9,$ and 11.1 . An approximate scale along the k axes, in units of 10^6 m^{-1} , is shown.

Large scattering peaks, with the peak points lying roughly parallel to the flow direction, are a feature of both the simulation and the experimental systems. However, the peaks are fairly broad, and thus orientation of the peaks themselves cannot be uniquely identified. The amplitudes of the peaks decrease, moderately, with increasing shear rate as we move from the purely shear thinning regime into the transitional region of the rheology curve (cf. Fig. 3).

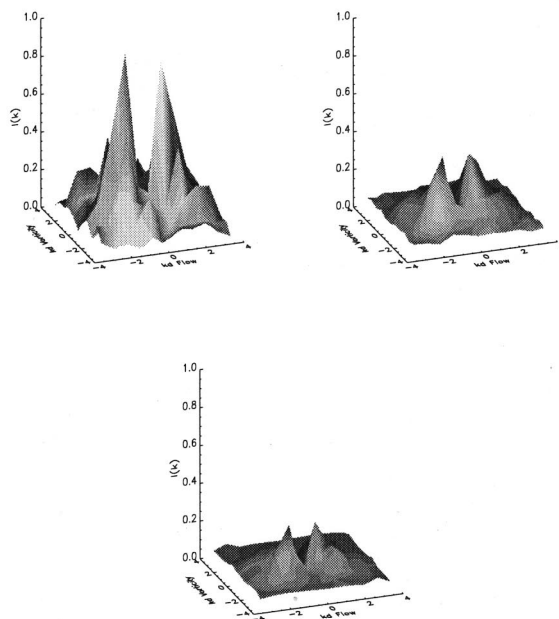
We have not attempted to compare data at zero-shear rate in Fig. 14 as the zero-shear system, in particular, is largely dependent on preparation (history). For the gel-forming system of Verduin *et al.* (1996), the zero-shear system is prepared at high temperatures and then cooled to the experimental temperature *without* shearing [Dhont (1998)]. However, the zero-shear system in Verduin *et al.* (1996) exhibits isotropic scattering peaks which suggest long range structure in the quiescent gel.

Therefore we find that without any detailed knowledge of the functional form of the interaction potential of the experimental system (other than the fact they represent gel-forming systems), our simulation data capture some of the qualitative features of the experimental system; the maximum pre-peak heights in $I(\mathbf{k})$ decrease with increasing shear rate, over the range of shear rates studied, from left to right in the figure.

IV. CONCLUSIONS

The rheology of aggregating and nonaggregating systems has been compared over a wide range in shear rate in the concentrated regime. The aggregating system is seen to experience a large viscous enhancement over the equivalent hard sphere system during the shear thinning regime. Although the attractive forces are not explicitly responsible for this modified rheological behavior, we find that the reason for this enhancement is manifested in the increased viscous contribution from the repulsive colloid forces when attractive forces are present. The microstructural mechanisms responsible for shear thinning rheology must be dominated by the close approach of particle surfaces through which the surface coat interactions contribute significantly to the shear stress. We also find that the transition to order at high shear rates is inhibited due to the aggregating forces, though the particular type of order achieved appears to be dependent on volume fraction in this concentrated regime.

Simulation Data



Experimental Data

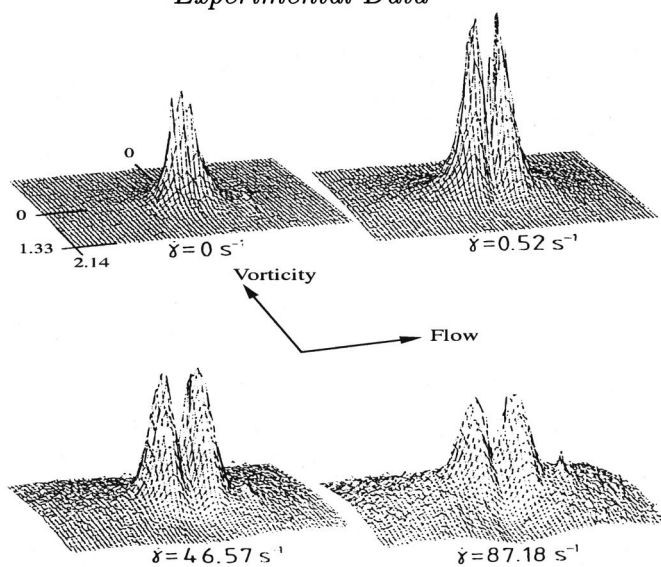


FIG. 14. Comparison between $I(\mathbf{k})$ from the simulation scattering data (top three shaded formats) for $Pe = 0.05, 5.0,$ and $10.0,$ with experimentally determined light-scattering studies (bottom four mesh plots). Reprinted with permission from Langmuir **12**, 2953 (1996), Copyright 1996 American Chemical Society) on a model power law, shear thinning adhesive colloidal system, at $Pe = 0.0, 0.07, 5.9,$ and $11.1.$

The aggregating system exhibits power law shear thinning behavior over a wide range of shear rates. The normal stress differences vary very little (and remain close to zero) during the shear thinning regime. This power law behavior is found to be universal in the context of the simulations at high colloid concentrations, and the value of the power law index computed here is comparable to values from similar experimental systems at comparable volume fractions. In this regime, the approximate functional dependencies of the viscosity on both the colloid volume fractions and the strength of the interaction potential were determined. Consequently, a full constitutive equation is given for the system in the shear thinning regime. As N_1 and N_2 are hard to measure in experiment, we hope that Eq. (15) may provide a useful constitutive relation for continuum models.

Configuration snapshots and computed scattering data of the system suggest that during the shear thinning regime, the system microstructure exhibits liquid-like short range order. However, the presence of pre peaks at small values of wave number, $kd \approx 1.0$, which are only seen during shear thinning systems, indicates the presence of intermediate range order due to longer ranged correlations. These are so far undetermined [Silbert (1998)], but such features are not observed in shear thinning hard spheres [Heyes and Mitchell (1995)]. However, a cautious comparison with recent experimental work shows that the simulation data do capture some of the qualitative features observed in experimental scattering data on systems which may crudely be considered a close comparison.

ACKNOWLEDGMENTS

This research was supported by the external Unilever colloid physics program and the BBSRC food directorate, together with Dalgety plc., and the EPSRC under Grant No. GR/L21747. The authors would like to thank R. S. Farr, K. G. Soga, and, in particular, R. Buscall for many useful discussions.

References

- Ackerson, B. J., "Shear induced order and shear processing of model hardsphere suspensions," *J. Rheol.* **34**, 553–590 (1990).
- Ball, R. C. and J. R. Melrose, "A simulation technique for many spheres in quasi-static motion under frame-invariant pair drag and Brownian forces," *Physica A* **247**, 444–472 (1997).
- Barnes, H. A., J. F. Hutton, and K. Walters, *An Introduction to Rheology*. Number 3 in Rheology Series (Elsevier, New York, 1989).
- Baxter-Drayton, Y. and J. F. Brady, "Brownian electrorheological fluids as a model for flocculated dispersions," *J. Rheol.* **40**, 1027–1056 (1997).
- Bender, J. W. and N. J. Wagner, "Optical measurements of the contributions of colloidal forces to the rheology of concentrated suspensions," *J. Colloid Interface Sci.* **172**, 171–184 (1995).
- Bilodeau, R. R. and D. W. Bousfield, "Shear-thinning predictions from particle motion modeling," *J. Rheol.* **42**, 743–764 (1998).
- Boersma, W. H., J. Laven, and H. N. Stein, "Computer-simulations of shear thickening of concentrated dispersions," *J. Rheol.* **39**, 841–860 (1995).
- Bossis, G. and J. F. Brady, "Dynamic simulation of sheared suspensions. 1. General-method," *J. Chem. Phys.* **80**, 5141–5154 (1984).
- Bossis, G. and J. F. Brady, "The rheology of Brownian suspensions," *J. Chem. Phys.* **91**, 1866–1874 (1989).
- Brady, J. F., "The rheological behaviour of concentrated colloidal dispersions," *J. Chem. Phys.* **99**, 567–581 (1993).
- Brady, J. F. (personal communications, 1998).
- Buscall, R., J. I. McGowan, and A. J. Morton-Jones, "The rheology of concentrated dispersions of weakly attracting colloidal particles with and without wall slip," *J. Rheol.* **37**, 621–641 (1993).
- Catherall, A. A. (Private communications, 1998).
- Chen, D. and M. Doi, "Simulation of aggregating colloids in shear flow. II." *J. Chem. Phys.* **91**, 2656–2663 (1989).

- Clarke, S. M., A. R. Rennie, and R. H. Ottewill, "Structure of dispersions under shear," in *Modern Aspects of Colloidal Dispersions*, edited by R. H. Ottewill and A. R. Rennie (Kluwer, Dordrecht, 1998), p. 113.
- de Kruij, C. G., E. M. F. van Lersel, A. Vrij, and W. B. Russel, "Hard sphere colloidal dispersions: Viscosity as a function of shear rate and volume fraction," *J. Chem. Phys.* **83**, 4717–4725 (1985).
- de Rooij, R., A. A. Potanin, D. van den Ende, and J. Mellema, "Steady shear viscosity of weakly aggregating polystyrene latex dispersions," *J. Chem. Phys.* **99**, 9213–9223 (1993).
- Dhont, J. K. G. (personal communications, 1998).
- Doi, M., D. Chen, and K. Saco, *Ordering and Organising in Ionic Solutions* (World Scientific, Singapore, 1987), p. 482.
- Dratler, D. I. and W. R. Schowalter, "Dynamic simulations of suspensions of non-Brownian hard spheres," *J. Fluid Mech.* **325**, 53–77 (1996).
- Durlofsky, L., J. F. Brady, and G. Bossis, "Dynamic simulation of hydrodynamically interacting particles," *J. Fluid Mech.* **180**, 21–49 (1982).
- Einstein, A., *Investigations on the Theory of Brownian Movement* (Dover, New York, 1956).
- Farr, R. S., Ph.D. thesis, University of Cambridge, Cambridge, U. K..
- Farr, R. S., J. R. Melrose, and R. C. Ball, "Kinetic theory of jamming in hard-sphere startup flows," *Phys. Rev. E* **55**, 7203–7211 (1997).
- Götzelmann, B., R. Evans, and S. Dietrich, "Depletion forces in fluids," *Phys. Rev. E* **57**, 6785–6800 (1998).
- Happel, J. and H. Brenner, *Low Reynolds Number Hydrodynamics* (Martinus Nijhoff, The Hague, 1983).
- Haw, M. D., W. C. K. Poon, and P. N. Pusey, "Direct observation of oscillatory-shear-induced order in colloidal suspensions," *Phys. Rev. E* **57**, 6859–6864 (1998).
- Heyes, D. M. and P. J. Mitchell, "Non-equilibrium molecular and Brownian dynamics simulations of shear thinning of inverse power fluids," *Mol. Phys.* **84**, 261–280 (1995).
- Huang, H. and C. M. Sorensen, "Shear effects during the gelation of aqueous gelatin," *Phys. Rev. E* **53**, 5075–5078 (1996).
- Hunter, R. J., *Foundations of Colloid Science II* (Cambridge University Press, Cambridge, England 1992).
- Krieger, I. M., "Rheology of monodisperse lattices," *Adv. Colloid Interface Sci.* **3**, 111 (1972).
- Lees, A. W. and S. F. Edwards, "The computer study of transport processes under extreme conditions," *J. Phys. C* **5**, 1921–1929 (1972).
- Lionberger, R. A., "Shear thinning of colloidal dispersions," *J. Rheol.* **42**, 843–863 (1998).
- Lionberger, R. A. and W. B. Russel, "A Smoluchowski theory with simple approximations for hydrodynamic interactions in concentrated dispersions," *J. Rheol.* **41**, 399–425 (1992).
- Melrose, J. R. and R. C. Ball, "The pathological behaviour of sheared hard-spheres with hydrodynamic interactions," *Europhys. Lett.* **32**, 535–540 (1995).
- Melrose, J. R. and D. M. Heyes, "Simulations of electrorheological and particle mixture suspensions—agglomerate and layer structure," *J. Chem. Phys.* **98**, 5873–5886 (1993).
- Morin, B. and D. Ronis, "Disorder and order in sheared colloidal suspensions," *Phys. Rev. E* **54**, 576–587 (1996).
- Patel, P. D. and W. B. Russel, "The rheology of polystyrene lattices phase separated by dextran," *J. Rheol.* **31**, 599–618 (1987).
- Phung, T. N., J. F. Brady, and G. Bossis, "Stokesian dynamics simulations of Brownian suspensions," *J. Fluid Mech.* **313**, 181–207 (1996).
- Potanin, A. A., R. de Rooij, D. van den Ende, and J. Mellema, "Microrheological modeling weakly aggregated dispersions," *J. Chem. Phys.* **14**, 5845–5853 (1995).
- Potanin, A. A. and W. B. Russel, "Fractal model of consolidation of weakly aggregated colloidal dispersions," *Phys. Rev. E* **53**, 3702–3709 (1996).
- Rudhardt, D., C. Bechinger, and P. Leiderer, "Direct measurement of depletion potentials in mixtures of colloids and nonionic polymers," *Phys. Rev. Lett.* **81**, 1330–1333 (1998).
- Rueb, C. J. and C. F. Zukoski, "Viscoelastic properties of colloidal gels," *J. Rheol.* **41**, 197–218 (1997).
- Russel, W. B., D. A. Saville, and W. R. Schowalter, *Colloidal Dispersions* (Cambridge University Press, Cambridge, England 1989).
- Silbert, L. E., Ph.D. thesis, University of Cambridge, Cambridge, U.K.
- Silbert, L. E., J. R. Melrose, and R. C. Ball, "Colloidal microdynamics: Pair-drag simulations of concentrated, aggregated systems," *Phys. Rev. E* **56**, 7067–7077 (1997).
- Toivakka, M., D. Eklund, and D. W. Bousfield, "Prediction of suspension viscoelasticity through particle motion modeling," *J. Non-Newtonian Fluid Mech.* **56**, 49–64 (1995).
- Verduin, H., B. J. de Gans, and J. K. G. Dhont, "Shear induced structural changes in a gel-forming suspension studied by light scattering and rheology," *Langmuir* **12**, 2947–2955 (1996).
- Verduin, H. and J. K. G. Dhont, "Phase diagram of a model adhesive hard-sphere dispersion," *J. Colloid Interface Sci.* **172**, 425–437 (1995).
- Wessel, R. and R. C. Ball, "Fractal aggregates and gels in shear flow," *Phys. Rev. A* **46**, R3008–R3011 (1992).

West, A. H. L., J. R. Melrose, and R. C. Ball, "Computer simulations of the breakup of colloid aggregates," *Phys. Rev. E* **49**, 4237–4249 (1994).

Whittle, M. and E. Dickinson, "Stress overshoot in a model particle gel," *J. Chem. Phys.* **107**, 10191–10200 (1997).

Wolthers, W., Ph.D. thesis, University of Twente, The Netherlands.